Robust Design of Piezoelectric Energy Harvesting Devices using Multiobjective Optimization Techniques

Paulo H. Martins[1], Marcelo A. Trindade[1], Paulo S. Varoto[1]

[1]*Department of Mechanical Engineering, University of São Paulo*
Av. Trabalhador São-carlense, 400, 13566-590, São Carlos, SP, Brazil
paulo.martins@usp.br, trindade@sc.usp.br, varoto@sc.usp.br

Abstract. For the robust design of piezoelectric energy harvesting devices, it is necessary to estimate the mean and variance of the harvesting performance due to uncertainties in device parameters. This is done here using Polynomial Chaos Expansions (PCE). Aiming at overcoming the total computational cost required for the robust optimization, a discussion on the selection of the most relevant uncertain parameters and on the degree and convergence of the PCE is performed. Then, with a satisfactory modeling choice, a multi-objective optimization using Non-dominated Sorting Genetic Algorithm (NSGA-II) is performed to determine Pareto fronts and box-plots that allow to choose the harvesting devices with better compromise between performance mean and dispersion.

Keywords: energy harvesting, uncertainties, piezoelectric sensors, robust devices, optimization

1 Introduction

Alternative energy sources have been studied in response to the high demand for energy in recent years. In this sense, electrical energy can be harvested from mechanical vibrations using resonant devices with piezoelectric elements that convert strain energy into electrical energy and electrical circuits that harvest and store this energy for later use in different applications. Figure 1 shows a typical resonant piezoelectric energy harvesting device in which an applied harmonic displacement $w_0(t)$ at the clamp induces vibration and, thus, deformation of the cantilever beam and piezoelectric patch. The tip mass m_b is used to tune the resonance frequency of the device with the base excitation frequency, producing the resonance phenomenon and maximizing the energy harvested. The piezoelectric patch is coupled to the beam through an adhesive layer and connected to an electrical resistance R_c, which is used as a proxy of the real harvesting circuit to estimate the energy available to be harvested.

Due to the small amount of energy typically available for conversion, it is important that the design of devices include an optimization process to maximize the energy harvested [1]. Optimization methods seek to find the parameters which minimize/maximize certain functions subject to equality or inequality constraints. They can be classified in mathematical programming and modern or non-traditional techniques, such as meta-heuristic methods [2]. Unlike mathematical programming methods based on differential calculus, meta-heuristics methods are generally less susceptible to initial guesses and local optima and do not require continuous or differentiable objective functions. They are also particularly useful for problems requiring a multi-objective optimization.

Although optimization methods can be used to design energy harvesting devices with optimal nominal performance, it is also important to consider the effect of uncertainties in device parameters and/or in the environment [3]. In this vein, optimization under uncertainties such as robust design optimization (RDO) seeks to find solutions that are less sensitive to relevant sources of variability [4]. The mean and variance functions are interesting alternatives to estimate the variability or robustness of a solution in robust design optimization. Different possibilities for the estimation of mean and variance have been presented such as Monte Carlo Simulation, Taylor series, Karhunen–Loève and Polynomial Chaos Expansions [4, 5].

After estimating mean and variance, they can be considered as competing objective functions in multi-objective optimization. For the energy harvesting problem, for instance, the mean performance, or mean energy harvested, must be maximized and its dispersion or variability must be minimized at the same time. Multi-objective optimization methods converge to a set of many solutions which are usually shown in a plot known as Pareto front,

unlike the optimization of a single function which returns one optimal solution [6]. The Pareto front can distinguish the type of problem studied as convex or non-convex where one goal for each solution cannot be improved without worsening another goal. In particular, a multi-objective method known as Non-dominated Sorting Genetic Algorithm (NSGA-II) find many solutions in a Pareto front by choosing the individuals in each run of the simulation that best represent the front [7]. Then, the analyst may check the solutions found and, based on any subjective criteria, choose an appropriate solution for the particular problem.

In this work, an energy harvesting device with uncertainties in certain parameters is modeled using the finite element method and a harmonic displacement is applied to the clamp to induce vibrations and, thus, harvested energy. Using the frequency response function (FRF) of electric power output, the mean and the variance are estimated using Polynomial Chaos Expansions. Then, the NSGA-II multi-objective optimization method is used to find the best device designs that simultaneously maximize the mean harvested energy and minimize its dispersion.

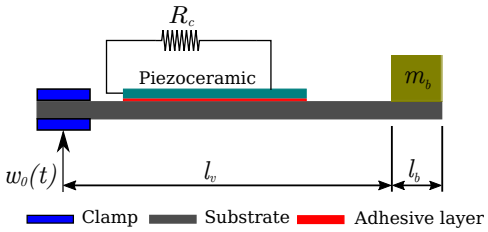

Figure 1. Typical model of energy harvesting devices based on resonating cantilever beams.

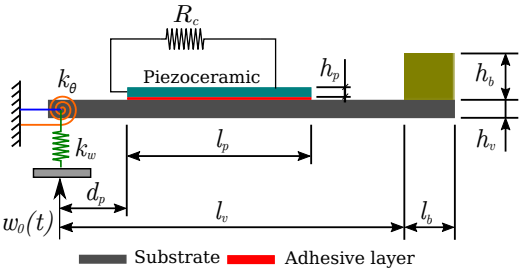

Figure 2. Schematic representation of the energy harvesting resonant device with imperfect clamp.

2 Finite element model of a piezoelectric energy harvesting device

The finite element model for the energy harvesting device is based on [8]. The model consists of three layers, two external or face layers that represent the host beam (substrate) and the piezoelectric patch, following Bernoulli-Euler beam theory, and one core or central layer that represent the adhesive (bonding) layer between substrate and patch, modeled using Timoshenko beam theory to allow expected shear strains. The piezoelectric material is considered orthotropic and entirely covered by electrodes. Figure 2 presents the device considered here to evaluate the harvested energy accounting for an imperfect clamp simulated by linear k_w and torsional k_θ springs. The geometric properties are summarized as follows: beam length l_v and height h_v, piezoelectric length l_p and height h_p, tip mass length l_b and height h_b and distance between piezoelectric patch and clamp d_p. A harmonic displacement $w_0(t)$ is applied to the clamp causing vibrations and the harvestable energy is estimated through the power dissipated in the equivalent electrical resistance R_c. The equations of motion are written as

$$\mathbf{M}_{rr}\ddot{\mathbf{u}}_r + \mathbf{K}_{rr}\mathbf{u}_r - \bar{\mathbf{K}}_{me}q_c = \mathbf{m}^\star\ddot{w}_0(t), \tag{1}$$

$$R_c\dot{q}_c - \bar{\mathbf{K}}_{me}^t\mathbf{u}_r + \bar{K}_e q_c = 0, \tag{2}$$

where $\mathbf{M}_{rr}$, $\mathbf{K}_{rr}$, $\bar{\mathbf{K}}_{me}$ and $\bar{\mathbf{K}}_e$ are matrices of mass and mechanical, piezoelectric and dielectric stiffnesses, respectively. $\mathbf{u}_r$ is a vector of displacements relative to the base displacement, $w_0(t) = \tilde{w}_0 e^{i\omega t}$, q_c is the electrical charge induced in the piezoelectric patch and $\mathbf{m}^\star$ is a column vector with mass elements. The model is reduced by projecting onto a truncated modal basis such that $\mathbf{u}_r \approx \boldsymbol{\phi}\boldsymbol{\alpha}_r$, in which the modal basis $\boldsymbol{\phi}$ is obtained by solving the undamped eigenvalue problem $[-\omega^2\mathbf{M}_{rr} + \mathbf{K}_{rr}]\boldsymbol{\phi} = 0$. By also considering a modal damping matrix $\boldsymbol{\Lambda}$, (1) and (2) are rewritten as

$$(-\mathbf{I}\omega^2 + j2\omega\boldsymbol{\Lambda}\boldsymbol{\Omega} + \boldsymbol{\Omega}^2)\tilde{\boldsymbol{\alpha}}_r - \mathbf{K}_p\tilde{q}_c = \boldsymbol{\phi}^t\mathbf{m}^\star(-\omega^2\tilde{w}_0), \tag{3}$$

$$(j\omega R_c + \bar{K}_e)\tilde{q}_c - \mathbf{K}_p^t\tilde{\boldsymbol{\alpha}}_r = 0, \tag{4}$$

where $\mathbf{I} = \boldsymbol{\phi}^t\mathbf{M}_{rr}\boldsymbol{\phi}$, $\boldsymbol{\Omega}^2 = \boldsymbol{\phi}^t\mathbf{K}_{rr}\boldsymbol{\phi}$ and $\mathbf{K}_p = \boldsymbol{\phi}^t\mathbf{K}_{me}$. $\tilde{\boldsymbol{\alpha}}_r$ and $\tilde{q}_c$ are the modal displacements and circuit electric charges, respectively. Considering the relations between voltage, current and charges in the circuit, such that $V_c = R_c i_c$ and $i_c = \dot{q}_c$, it is possible to define the FRF of voltage output per unit base acceleration as follows

$$G_{V\ddot{w}_0}(\omega) = j\omega R_c\mathbf{K}_p^t\mathbf{D}^{-1}\boldsymbol{\phi}^t\mathbf{m}^\star, \tag{5}$$

where $\mathbf{D} = (j\omega R_c + \bar{K}_e)(-\mathbf{I}\omega^2 + j2\omega\boldsymbol{\Lambda}\boldsymbol{\Omega} + \boldsymbol{\Omega}^2) - \mathbf{K}_p\mathbf{K}_p^t$. Similarly, defining the power dissipated in the resistive circuit as $P = V_c^2/R_c$, the FRF of power output per unit squared base acceleration $G_{P\ddot{w}_0}(\omega)$ is written as

$$G_{P\ddot{w}_0}(\omega) = (G_{V\ddot{w}_0}(\omega))^2/R_c. \tag{6}$$

The latter (6) will be used as performance metric to design devices, targeting both maximization of the mean harvested power and minimization of its dispersion. For that, it is necessary to estimate its mean and variance, which will be later used in a multi-objective optimization.

3 Mean and variance estimation

For a computational model $\mathcal{M}$ with random input vector $\mathbf{X}$, the random response is defined as $Y \equiv \mathcal{M}(\mathbf{X})$. The Polynomial Chaos Expansions (PCE) allows to estimate the quantity of interest Y using [9]

$$Y \equiv \mathcal{M}(\mathbf{X}) = \sum_{\boldsymbol{\varrho} \in \mathbb{N}^M} c_{\boldsymbol{\varrho}} \Psi_{\boldsymbol{\varrho}}(\mathbf{X}), \tag{7}$$

where $c_{\boldsymbol{\varrho}}$ and $\Psi_{\boldsymbol{\varrho}}(\mathbf{X})$ are deterministic coefficients and multivariate orthonormal polynomials, respectively, associated with the multi-index $\boldsymbol{\varrho}$. Details for finding the multi-index, which is a list of integers with the sum of terms inferior or equal to the polynomial degree, can be found in [9]. Then, the multi-index notation is defined as $\boldsymbol{\varrho} = (\varrho_1, \varrho_2, \cdots, \varrho_M)$, $\varrho_i \in \mathbb{N}$, with M random variables in the computational model. By means of the multi-index $\boldsymbol{\varrho}$, the multivariate polynomial is defined as

$$\Psi_{\boldsymbol{\varrho}}(\boldsymbol{x}) \stackrel{\text{def}}{=} \prod_{i=1}^{M} \psi_{\varrho_i}^{(i)}(x_i), \tag{8}$$

where $\psi_{\varrho_i}^{(i)}$ is the univariate polynomial associated with the integer ϱ_i. The probability density function of each random variable X_i determines the corresponding univariate polynomial such as Hermite, Legendre and Laguerre polynomials for normal, uniform and gamma variables, respectively. It is also important to use the standardized random variable X_i to compute multivariate polynomials.

The length of a multi-index $\boldsymbol{\varrho}$ corresponds to the total degree of the multivariate polynomial, defined as

$$\boldsymbol{\varrho} \equiv \|\varrho\|_1 = \varrho_1 + \varrho_2 + \cdots \varrho_M. \tag{9}$$

The sum of terms of (9) is limited to the degree of polynomial chosen according to the set $\mathcal{A}^{M,p} = \{\boldsymbol{\varrho} \in \mathbb{N}^M \ : \ |\boldsymbol{\varrho}| \leq p\}$, allowing to truncate (7) so that

$$Y \equiv \mathcal{M}(\mathbf{X}) \approx \sum_{\boldsymbol{\varrho} \in A} c_{\boldsymbol{\varrho}} \Psi_{\boldsymbol{\varrho}}(\mathbf{X}). \tag{10}$$

The cardinality of the set $\mathcal{A} = \mathcal{A}^{M,p}$ determines the number of terms in (10), which can be found according to [9]. Next, the coefficients can be calculated using the least-square minimization by considering the argument that minimizes the mean square error between the computational model and the truncated polynomial. For this purpose, a drawing of random sample $\mathcal{X} = \{\boldsymbol{x}^{(i)}, \ i = 1, \cdots, n\}$ is performed using Monte Carlo Simulation (MCS), Latin Hypercube Sampling (LHS) and quasi-random sequence via Halton or Sobol methods for sampling. Thus, the sampled model responses are

$$\mathcal{Y} = \{y^{(1)} = \mathcal{M}(\boldsymbol{x}^{(1)}), \cdots, \boldsymbol{y}^{(n)} = \mathcal{M}(\boldsymbol{x}^{(n)})\}^T. \tag{11}$$

The polynomial bases are used to determine the following set

$$\mathbf{A} = \{\mathbf{A}_{ij} \stackrel{\text{def}}{=} \Psi_j(\boldsymbol{x}^{(i)}), \ i = 1, 2, \cdots, n, \ j = 1, 2, \cdots, \text{card}(\mathcal{A})\}. \tag{12}$$

where $\text{card}(\mathcal{A})$ is the cardinality of set $\mathcal{A}$. Then, the coefficients of the expansion are evaluated from

$$\hat{\boldsymbol{c}} = (\mathbf{A}^T \mathbf{A})^{-1} \mathbf{A}^T \mathcal{Y}. \tag{13}$$

The mean and variance of the computational model response is estimated from the coefficients of the PCE as

$$\mu_{\hat{Y}} = \mathbb{E}[\hat{Y}] = \mathbb{E}[\sum_{\boldsymbol{\varrho} \in A} \hat{c}_{\boldsymbol{\varrho}} \Psi_{\boldsymbol{\varrho}}(\mathbf{X})] = \hat{c}_0, \tag{14}$$

$$\sigma_{\hat{Y}}^2 \stackrel{\text{def}}{=} \text{Var}[\hat{Y}] = \mathbb{E}\left[(\hat{Y} - \hat{c}_0)^2\right] = \sum_{\substack{\boldsymbol{\varrho} \in A \\ \boldsymbol{\varrho} \neq 0}} \hat{c}_{\boldsymbol{\varrho}}^2. \tag{15}$$

For instance, (14) and (15) can be used to estimate the mean and variance of the response of power output according to (6) for given distributions and realizations of the uncertain input parameters and values of the other model parameters considered as deterministic. These estimations are then used as objective functions in a multi-objective optimization strategy.

4 Robust optimization using NSGA-II

The Non-dominated Sorting Genetic Algorithm (NSGA-II) is a method based on the classical genetic algorithm to solve problems with different objective functions simultaneously. For this reason, a population of points in each run of the algorithm is chosen in order to converge towards the Pareto front. In the convergence procedure, the method seeks multiple non-dominated solutions assigning fitness to the population members and trying to ensure the diversity of points in the final solutions [7].

In the genetic algorithm (GA), the convergence process is divided into stages of reproduction, crossover and mutation based on biological evolution concepts [2]. The variables are manipulated using individuals and a fitness function is evaluated to select the best individuals. By means of probabilistic concepts, the best individuals are selected at the reproduction stage and copies are created to form the mating pool. After this stage, part of the population from the mating pool is chosen and the crossover operator is applied by combining portions of the individuals aiming at producing offspring individuals with better fitness (objective function) values. Finally, the mutation operator is implemented by modifying certain characteristics (properties) of the individuals according to a specified probability. These steps are repeated for a number of generations (iterations) to find the optimal characteristics (design variables) that minimize or maximize a specific objective function.

The stages presented in the genetic algorithm are used in the NSGA-II to find non-dominated solutions and to ensure the diversity in the population. Thus, the first procedure is to rank the individuals by dividing the solutions in fronts or ranks, which are chosen according to the dominance concept. For instance, a hypothetical population can divided in rank 1, rank 2 and rank 3 so that the individuals of rank1 are closer to the optimum Pareto front and should be preferred in the non-dominance procedure. Then, for individuals in the same rank, the diversity of the population is preserved by considering solutions in a less crowded area with the help of an operator that measures the crowding distance.

The initial population with N individuals in NSGA-II is ranked and the operators of reproduction, crossover and mutation are applied to create an offspring population. The new population, which consists of $2N$ individuals, are sorted according to the dominance concept in the best ranks. Also, the crowding distance operator is applied to the individuals in the same rank. Hence, the population is truncated and the best solutions of N individuals are separated, ending the iteration. This process is repeated in order to find the Pareto-optimal solutions based on the number of iterations determined by the end-user.

5 Procedure for designing robust energy harvesting devices

The design strategy for robust energy harvesting devices consists of: i) defining the design and uncertain variables; ii) estimating the mean and variance of the power output FRF; and iii) applying the multi-objective optimization method. This procedure aims to maximize the mean and minimize the dispersion of the power output (6) using the PCE method by (14) and (15).

First, the beam length and electrical resistance are chosen as design variables and stored in the vector $\boldsymbol{x}_d = \{l_v, R_c\}$ (Figure 2). Then, the uncertain variables are chosen as the linear k_w and torsional k_θ clamping springs, electrical resistance R_c, effective damping ζ of the device, and height h_c and Young's Modulus E_c of the adhesive layer. These variables are stored in the vector $\boldsymbol{x}_u = \{k_w, k_\theta, \zeta, R_c, h_c, E_c\}$. For all uncertain variables, the Gamma probability distribution function is considered with shape parameter $\alpha = (\mu/\sigma)^2 = 1/\delta^2$ and scale parameter $\beta = \sigma^2/\mu = \mu\delta^2$, where μ, σ and δ state, respectively, as the mean, standard deviation and relative dispersion. These being defined for each uncertain variable, it is possible to evaluate the corresponding parameters α and β and, thus, generate samples (realizations) of each variable following the chosen distribution. For all other model input parameters, that are not design or uncertain variables, fixed nominal (deterministic) values are set.

Since the main purpose of the energy harvesting device design optimization is to maximize the harvested power output, the device resonance frequency must be tuned to the excitation frequency. This is done by internally evaluating the tip mass, through its height h_b, for a given set of device parameters so that the resonance frequency matches the pre-defined target frequency. Particularly, the FRF of power output indicated by (6) is evaluated for given vectors of design variables $\boldsymbol{x}_p$, uncertain variables $\boldsymbol{x}_u$ and excitation frequency ω_e such that

$$f(\boldsymbol{x}_p, \boldsymbol{x}_u) = G_{P\ddot{w}_0}(\boldsymbol{x}_p, \boldsymbol{x}_u, \omega_e). \tag{16}$$

Before applying the multi-objective optimization method, reference values for the mean μ_{ref} and standard deviation σ_{ref} are estimated by Monte Carlo Simulation with a larger number of samples for a particular set of design variables. This is done to enable the convergence verification of mean and dispersion estimation and corresponding selection of the minimum number of samples required for satisfactory convergence.

Then, the smaller number of samples is used to verify which uncertain variables have the most influence on the output dispersion. For that, the mean μ_f and dispersion δ_f power output (16) are estimated via MCS when eliminating one uncertain variable at a time. This is done by set the nominal value to that variable while others are sampled. The mean and dispersion estimations are then compared to the reference value, obtained when all uncertain variables are sampled. For instance, the mean and dispersion ignoring the uncertain variable k_w are denoted as $\mu_{\bar{k_w}}$ and $\delta_{\bar{k_w}}$. Whenever an uncertain variable has smaller influence on the mean and dispersion, the PCE method may be applied with a smaller number of uncertain variables, which helps improving convergence and reducing the computational cost of the optimization.

For a given design solution, represented by its corresponding design variables $\boldsymbol{x}_d = \{l_v, R_c\}$, and sampling N realizations of the uncertain variables $\boldsymbol{x}_u = \{k_w, k_\theta, \zeta, R_c, h_c, E_c\}$, it is possible to evaluate the corresponding realizations of the objective function $f(\boldsymbol{x}_d, \boldsymbol{x}_u)$ and, thus, to estimate its mean and standard deviation. Alternatively, the Latin Hypercube Sampling (LHS) is used with MCS to improve the sampling process by dividing every variable into subsets with equal probability and selecting only one sample in each stratum [10].

After choosing the most relevant uncertain variables in vector $\boldsymbol{x}_u$, the PCE with different degrees is used to estimate the mean and variance for the particular design variables with various number of samples. This is done to assess the minimum degree and number of samples for the PCE that yield a satisfactorily small error relative to the MCS reference estimations. To compute the PCE coefficients, the samples of uncertain variables in (11) are obtained with a quasi-random sequence using the Halton procedure based on [11]. Then, with the chosen degree and number of samples of the PCE to well estimate the mean and variance of the power output (16), these are used in the NSGA-II procedure to obtain the optimal solutions subjected to predefined choices for the number of individuals and iterations and lower and upper bounds for each design variable $\boldsymbol{x}_d^L \leq \boldsymbol{x}_d \leq \boldsymbol{x}_d^U$.

6 Results and discussion

Experimental results for an energy harvesting device laboratory setup were used to verify and update the finite element model and its corresponding nominal parameters. The geometric properties of the experimental device are summarized as follows (according to Figure 2): $l_v = 74.7$ mm, $l_p = 73.$ mm, $l_b = h_b = 12.8$ mm, $h_p = 0.13$ mm, $d_p = 1.1$ mm and 12.8 mm of width for all parts. The tip mass is on top of a segment of the substrate, thus the total mass is estimated at 9.2 g and rotation inertia at 0.8 kg mm^2. A PZT-5A piezoceramic was considered with elastic stiffness constant $\bar{c}_{11}^E = 66.3$ GPa, piezoelectric constant $\bar{e}_{31} = 13.3$ C/m^2 and dielectric constant $\bar{\epsilon}_{33}^{\bar{\varepsilon}} = 12.3$ nF/m and density 7850 kg m^{-3}. For the substrate, aluminum was considered with Young's modulus 68 GPa and density 2700 kg m^{-3}. The Epoxy-based 3M Scotch-Weld DP-460 adhesive layer has Young's modulus 2 GPa and density 1126 kg m^{-3}. The damping factor of $\zeta = 1.1\%$ identified in experimental tests was also used in the numerical model. By using different electrical resistance values, numerical and experimental FRFs of voltage induced at the piezoelectric patch electrode and transverse acceleration output at tip mass were evaluated.

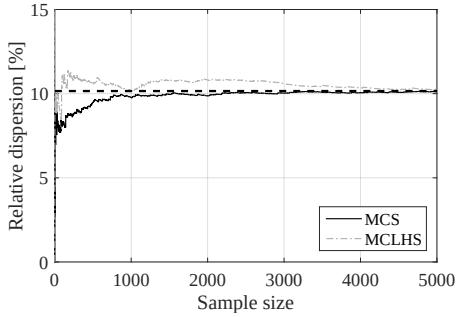

Figure 3. Convergence of MCS dispersion estimation.

Table 1. Output power mean μ and relative dispersion δ estimation removing one uncertain variable at a time.

	[mW/g^2]	$e_r(\%)$		[%]	$e_r(\%)$
$\mu_{\bar{k_w}}$	42.52	1.3	$\delta_{\bar{k_w}}$	8.66	14.7
$\mu_{\bar{k_\theta}}$	42.63	1.6	$\delta_{\bar{k_\theta}}$	8.23	18.9
$\mu_{\bar{\zeta}}$	41.88	0.2	$\delta_{\bar{\zeta}}$	9.48	6.6
$\mu_{\bar{R_c}}$	42.03	0.1	$\delta_{\bar{R_c}}$	10.04	1.0
$\mu_{\bar{E_c}}$	43.38	0.3	$\delta_{\bar{E_c}}$	9.76	3.8
$\mu_{\bar{h_c}}$	42.09	3.3	$\delta_{\bar{h_c}}$	7.50	26.1

The uncertain variables are defined with mean value and relative dispersions, making it possible to determine the shape and scale parameters for the Gamma distributions. First, the mean and variance of power output (16) were estimated with MCS for the case with $l_v = 75$ mm and $R_c = 100$ kΩ while previously defined values were kept for the other parameters. The mean (nominal) values and relative dispersions of the uncertain parameters are summarized as: $k_w = 50$ kN/m ($\delta_{k_w} = 30\%$), $k_\theta = 0.3$ kNm/rad ($\delta_{k_\theta} = 30\%$), $\zeta = 1.1\%$ ($\delta_\zeta = 10/3\%$), $R_c = 100$ kΩ ($\delta_{R_c} = 10\%$), $h_c = 0.08$ mm ($\delta_{h_c} = 10\%$), $E_c = 2.0$ GPa ($\delta_{E_c} = 50/3\%$). Thus, the reference

values for the mean and dispersion estimated using MCS with 10^6 samples were $\mu_{\text{ref}} = 41.964$ mW/g^2 and $\delta_{\text{ref}} = \sigma_{\text{ref}}/\mu_{\text{ref}} = 10.155\%$. Then, the convergence of dispersion estimation using MCS and MCS/LHS was verified and plotted in Figure 3. It indicates that 4000 samples should be accurate enough for both MCS and MCS/LHS methods.

Thus, this number of samples were used to evaluate the mean and dispersion excluding one variable at a time. These are given in Table 1 together with the relative error e_r with respect to the reference values μ_{ref} and δ_{ref}. While the error in estimation of the mean values is small in all cases, the error for the dispersion is much more important. From Table 1, one may conclude that the circuit resistance R_c and adhesive modulus E_c are the least important uncertain variables and, thus, could be removed from the set of uncertain variables, which was then reduced to $\boldsymbol{x}_u = \{k_w, k_\theta, \zeta, h_c\}$, noticing that R_c is still kept as one of the design variables.

In order to choose an adequate number of samples for the PCE with Halton sequence, the MCS was first applied with 10^4 samples for vector the $\boldsymbol{x}_u = \{k_w, k_\theta, \zeta, h_c\}$. The power output mean and relative dispersion resulted in 42.17 mW/g^2 and 9.62%, respectively, for the design variables set $\boldsymbol{x}_d = \{75 \text{ mm}, 100 \text{ k}\Omega\}$. Using these values as reference, the convergence in dispersion estimation of PCE with three different polynomial degrees was assessed and is shown in Figure 4. It indicates that a PCE of degree 3 converges faster to satisfactory error levels and, thus, a PCE-3 with 400 samples was chosen to estimate mean and dispersion in the multi-objective optimization with NSGA-II.

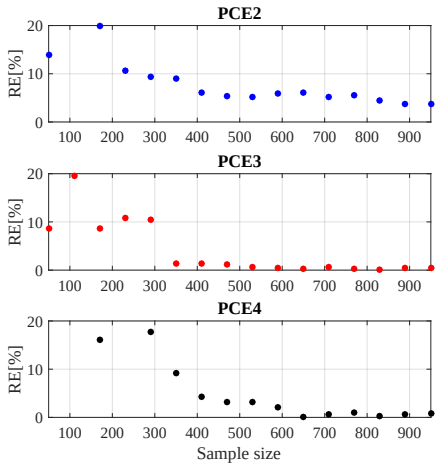

Figure 4. Convergence of PCE dispersion estimation.

Table 2. Design variables, μ and δ using NSGA-II.

Device	l_v (mm)	h_b (mm)	R_c (kΩ)	μ_Y (mW/g^2)	δ_Y (%)
1	65.0	18.6	66.9	57.7	9.10
2	65.0	18.5	53.4	57.5	8.77
3	65.8	17.9	48.4	56.2	8.64
4	67.1	16.9	43.8	54.0	8.48
5	69.4	15.5	48.3	50.9	8.23
6	71.5	14.2	44.0	47.9	7.99
7	73.1	13.3	42.2	45.8	7.84
8	75.9	11.9	41.1	42.5	7.60
9	79.1	10.5	40.7	39.0	7.37
10	84.2	8.5	36.7	34.4	7.08
11	85.0	8.3	36.7	33.7	7.04

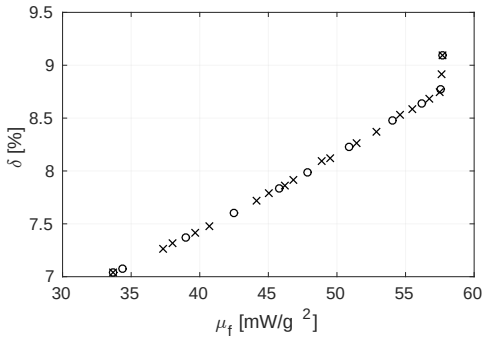

Figure 5. Pareto-front for δ and μ.

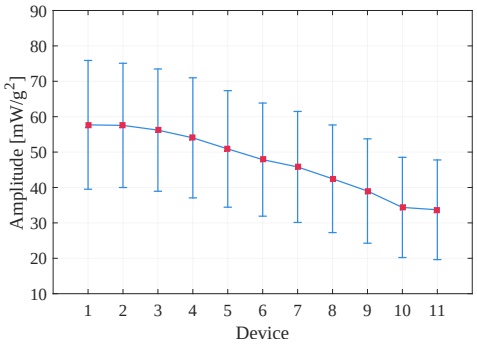

Figure 6. 4σ box-plot of harvested power.

Considering the lower and upper bounds of 65 mm $\leq l_v \leq$ 85 mm and 20 kΩ $\leq R_c \leq$ 400 kΩ for design variables, the NSGA-II multi-objective technique combined to a PCE of degree 3 (PCE-3) for the estimation of power output mean and dispersion was used to evaluate optimal solutions for a robust design. Figure 5 shows the Pareto front for the two objectives, mean harvested power (to be maximized) and its dispersion (to be minimized), found when applying NSGA-II with PCE-3. 30 individuals and 300 iterations were chosen leading to the devices that converged to the Pareto front shown in Figure 5.

Some selected devices, represented by crosses in Figure 5, and their corresponding performances are shown in Table 2. The first selected device has better performance (higher mean) while the last one is more robust (lower dispersion). It is noticeable that devices with shorter lengths, and hence larger tip masses, provide greater mean

harvested power while devices with greater lengths are more robust. Figure 6 presents a box-plot with a confidence interval of $\pm 2\sigma$ for the harvested power for the devices listed in Table 2. It may be helpful to compare the robust performance of the selected devices. For instance, it suggests that device 2 is better than device 1 since the worst case performance (lower-bound) is higher for device 2 while the mean performance is only marginally smaller. This occurs mainly by decreasing the electrical resistance, while the other parameters are nearly the same, as presented in Table 2. Other devices can be compared in terms of best and worst case performances using both box-plot and Pareto front and according to a subjective analysis to select an appropriate device.

7 Conclusions

This work has presented an analysis of the robust design of piezoelectric energy harvesting devices considering parametric uncertainties in the cantilever clamping, circuit resistance, damping factor, and adhesive thickness and modulus. A discussion on the selection of the most relevant uncertain parameters and on the degree and convergence of a Polynomial Chaos Expansion to estimate the harvested power mean and dispersion was performed. It was shown that the adhesive layer thickness and clamping stiffness are the most relevant uncertain parameters. Then, a multi-objective optimization using Non-dominated Sorting Genetic Algorithm (NSGA-II) was performed to determine Pareto fronts and box-plots that allow to choose the harvesting devices with better compromise between performance mean and dispersion. Results show that generally harvesting devices with larger tip masses lead to greater mean performance but also larger dispersion and, thus, are less robust. It was also observed that the robustness may be increased by reducing the effective resistance of the harvesting circuit.

Acknowledgements. Financial support of CNPq, through grants 309193/2014-1 and 309001/2018-8, and CAPES, through a doctoral scholarship, is gratefully acknowledged.

Authorship statement. The authors hereby confirm that they are the sole liable persons responsible for the authorship of this work, and that all material that has been herein included as part of the present paper is either the property (and authorship) of the authors, or has the permission of the owners to be included here.

References

[1] T. C. Godoy, M. A. Trindade, and J. F. Deü. Topological optimization of piezoelectric energy harvesting devices for improved electromechanical efficiency and frequency range. In *Proceedings of 10th World Congress on Computational Mechanics (WCCM), São Paulo*, pp. 4003–4016, 2014.
[2] S. S. Rao. *Engineering optimization: theory and practice*. John Wiley & Sons, 2009.
[3] V. R. Franco and P. S. Varoto. Parameter uncertainties in the design and optimization of cantilever piezoelectric energy harvesters. *Mechanical Systems and Signal Processing*, vol. 93, pp. 593–609, 2017.
[4] G. I. Schuëller and H. A. Jensen. Computational methods in optimization considering uncertainties–an overview. *Computer Methods in Applied Mechanics and Engineering*, vol. 198, pp. 2–13, 2008.
[5] H.-S. Beyer and B. Sendhoff. Robust optimization–a comprehensive survey. *Computer methods in applied mechanics and engineering*, vol. 196, n. 33-34, pp. 3190–3218, 2007.
[6] R. T. Marler and J. S. Arora. Survey of multi-objective optimization methods for engineering. *Structural and multidisciplinary optimization*, vol. 26, n. 6, pp. 369–395, 2004.
[7] K. Deb, A. Pratap, S. Agarwal, and T. Meyarivan. A fast and elitist multiobjective genetic algorithm: Nsga-ii. *IEEE Transactions on evolutionary computation*, vol. 6, n. 2, pp. 182–197, 2002.
[8] H. F. L. Santos. Structural vibration control using piezoceramics in extension and shear connected to hybrid active-passive circuits (in portuguese). Master's thesis, University of São Paulo, 2008.
[9] B. B. Sudret. Polynomial chaos expansions and stochastic finite element methods. *Risk and reliability in geotechnical engineering*, pp. 265–300, 2014.
[10] S. Poles and A. Lovison. A polynomial chaos approach to robust multiobjective optimization. In *Dagstuhl Seminar Proceedings*. Schloss Dagstuhl-Leibniz-Zentrum für Informatik, 2009.
[11] M. Kolář and S. F. O'Shea. Fast, portable, and reliable algorithm for the calculation of halton numbers. *Computers & Mathematics with Applications*, vol. 25, n. 7, pp. 3–13, 1993.